PHYSICAL REVIEW B **84**, 180201(R) (2011)

Structural phase transformation through defect cluster growth in Gd-doped ceria

Zhi-Peng Li,[1,*] Toshiyuki Mori,[1] Fei Ye,[2] Ding Rong Ou,[3] Jin Zou,[4,5] and John Drennan[5]

[1]*Global Research Center for Environment and Energy based on Nanomaterials Science, National Institute for Materials Science, Tsukuba, Ibaraki 305-0044, Japan*

[2]*Key Laboratory of Materials Modification, School of Materials Science and Engineering, Dalian University of Technology, 2 Linggong Road, Dalian, Liaoning 116024, People's Republic of China*

[3]*Laboratory of Fuel Cells, Dalian Institute of Chemical Physics, Chinese Academy of Sciences, 457 Zhongshan Road, Dalian, Liaoning 116023, People's Republic of China*

[4]*Division of Materials, The University of Queensland, St. Lucia, Brisbane, Queensland 4072, Australia*

[5]*Centre for Microscopy and Microanalysis, The University of Queensland, St. Lucia, Brisbane, Queensland 4072, Australia*

(Received 31 July 2011; published 7 November 2011)

Defect clusters with ordered structures in Gd-doped ceria have been verified by transmission electron microscopy. Atomistic simulation validates further the ordered structures and related pathway for cluster growth. A unique dumbbell structure formed with six oxygen vacancies in a ceria matrix has been identified as the building block for defect cluster growth and sequentially for the evolution from a F- to C-type lattice. As such, the phase transformation as established on the atomic scale occurs through this defect cluster growth.

DOI: 10.1103/PhysRevB.84.180201 PACS number(s): 81.30.Hd, 61.43.Bn, 68.37.Lp, 88.30.mj

Defect clusters, originating from aliovalent dopants and charge-compensating oxygen vacancies, are widely present in anion-deficient compounds.[1] Such defects have been extensively investigated in nonstoichiometrically stabilized zirconia or doped ceria due to their crucial roles in determining ionic conductivity of electrolytes in solid oxide fuel cells (SOFCs), the key technology to develop environmentally benign power sources.[2–4] The electrolyte ionic conductivity is provided by oxygen vacancies, the most mobile defects in oxygen-deficient oxides.[5] Contrary to the anticipation that ionic conductivity would increase monotonically with dopant concentration, investigations have revealed a saddle-shaped conductivity curve with the peak value at a certain critical doping level (10–20 at.%), far before reaching the maximum dopant solubility.[6] The mainstream explanation ascribes this nonmonotonic behavior to defect-defect interactions and defect ordering.[7,8] In stabilized zirconia, clusters that grow in ordered structures may enhance defect interactions, inhibit the diffusion of oxygen vacancies, and consequently decrease the conductivity.[9,10] Similarly, theoretical and numerical models have been developed for distributions and interactions of defects in rare-earth-doped ceria.[11] However, previous investigations only focused on the formation and interaction of small clusters (no larger than two oxygen vacancies).[11,12] Recently, Ye *et al*. proposed a helical chain model with up to four oxygen vacancies in Gd-doped ceria (GDC), but this model still fails to answer some critical questions.[13,14] It is well established that as the dopant concentration increases, the fluorite (F-type) lattice will gradually evolve through ordered fluorite-related structures to the C-type sesquioxide.[1,15] However, restricted by the low symmetry and nonconvergence trait of such a chain structure,[14] it is difficult to arrange the constituent positions and explain this phase transformation. Therefore, it is essential to explore with further research the interactions, ordered structures, and the related growth pathway of defect clusters. Insights gained from such studies can facilitate our understanding of the phase transformation at the atomic level, and consequently improve the physical and chemical properties of doped ceria for SOFC applications.

To fill the aforementioned gaps, this Rapid Communication provides, through experiment and atomistic simulation, evidences for defect cluster growth from a F- to C-type structure in GDC. The GDC nanopowders were synthesized by the ammonium carbonate coprecipitation method.[16] Calcined precursors were isostatically pressed and then sintered at 1400 °C. To explore defect cluster evolution as a function of the dopant concentration, high-resolution transmission electron microscopy (HRTEM), energy-filtering TEM (EFTEM), and selected-area electron diffraction (SAED) were performed on samples with different doping levels. Atomistic simulation was employed to investigate the growth of defect clusters. The simulation is based on the Born model,[17] where the short-range interactions are described by the Buckingham potential in the form of $E(r_{ij}) = A\exp(-r_{ij}/\rho) - Cr_{ij}^{-6}$ (r_{ij} for the atomic distances, and A, ρ, and C for adjustable parameters in Table I). The O^{2-} and Ce^{4+} ions are treated as polarizable, described by a shell mode,[18] with shell parameters Y $|e|$ and a harmonic spring of force constant k: $Y = -2.04$ and $k = 419.87$ eV/Å^2 for O^{2-}, and $Y = -0.20$ and $k = 291.75$ eV/Å^2 for Ce^{4+}.[19,20] To calculate the intrinsic defect energy, the Mott-Littleton two-region method was applied. Also, the binding energy E_b is calculated to investigate the preference and stability of defect clusters. It is described as $E_b = \Sigma E_{\text{isolated}} - E_{\text{cluster}}$, where $\Sigma E_{\text{isolated}}$ is the sum of the defect energy for all individual components and E_{cluster} is the entire defect energy of this cluster.

Figure 1 demonstrates the GDC microstructural evolution as a function of dopant concentration. To ensure comparability, all GDC samples were observed along the [110] zone axis. Figures 1(a) and 1(d) represent a typical fluorite structure. As the dopant concentration increases to 20 at.%, in addition to the sharp Bragg reflections arising from the fluorite lattice, other distinct diffuse scattering occurs [Fig. 1(e)], which can be attributed to nanosized domain formation [marked by the dashed lines in Fig. 1(b)]. Similar phenomena have been widely observed in other rare-earth-doped ceria.[21–23] For the 50GDC, larger areas with microstructures different from fluorite ceria appear [Fig. 1(c)]. Those extra diffraction spots

TABLE I. Short-range potential parameters.

Species	A (eV)	ρ (Å)	C (eVÅ^6)	References
Ce^{4+}-O^{2-}	1986.8	0.3511	20.40	19
Gd^{3+}-O^{2-}	1885.75	0.3399	20.34	19
O^{2-}-O	22764.3	0.149	45.83	20

in Fig. 1(f) can be indexed as the C type, verified by simulated electron diffraction patterns [Figs. 1(g) and 1(h)]. SAED patterns thus illustrate the evolution from the F- to C-type structure. The compositional and volume features of domains were further characterized by EFTEM elemental mapping. Such an investigation (Fig. 2) not only represents the inhomogeneous distributions of Ce and Gd in $Ce_{1-x}Gd_xO_{2-x/2}$ samples, but also illustrates the volume evolution of domains as a function of dopant concentration. In lightly doped ceria [$x = 0.1$, Fig. 2(a)], the compositional inhomogeneity is negligible. In 20GDC samples [Fig. 2(b)], the average volume ratio of domains is ~10.6%. It increases to ~19.1% in 30GDC [Fig. 2(c)]. Moreover, previous reports have attested that, as the dopant concentration increases, the level of oxygen vacancy ordering will also be enhanced, accompanied with domain formed in ordered structures.[22,23] However, the details of domain formation and related evolution process still remain unclear.

In general, an oxygen vacancy occupies the first, second, or third nearest-neighbor site with respect to the substituted dopant, separated by ⟨111⟩/4, ⟨113⟩/4, and ⟨133⟩/4, respectively. The Kröger-Vink notation is used to simplify the expression of the defect cluster. Various distributions of defects have been considered to assess the local stability of different configurations. For the smallest defect cluster ($1V_O^{\cdot\cdot}1Gd'_{Ce}$), the defect energy with oxygen vacancy ($V_O^{\cdot\cdot}$) located at the three nearest-neighbor sites is 48.04, 48.26, and 48.46 eV [Fig. 3(a)], indicating the first neighbor as the most preferred site. This is a more energetically favorable result since all dopants actually occupy the first neighbor site in the C-type structure, the end state in the structural evolution. The simplest neutralized cluster $1V_O^{\cdot\cdot}2Gd'_{Ce}$, with the highest binding energy, is shown in Fig. 3(b). For defect clusters containing more than two $V_O^{\cdot\cdot}$, the adjacent $V_O^{\cdot\cdot}-V_O^{\cdot\cdot}$ interaction usually occurs along either the ⟨110⟩/2 or ⟨111⟩/2 lattice vector.[19] Figure 3(c) represents the most stable $2V_O^{\cdot\cdot}4Gd'_{Ce}$ defect cluster. Calculations illustrate that the defects in any possible defect arrangements are neither isolated nor randomly distributed. All dopants prefer to occupy the site that is not only the first neighbor to its corresponding $V_O^{\cdot\cdot}$, but also the first or second neighbor to its nearby $V_O^{\cdot\cdot}$ to ensure the lowest overall defect energy. This criterion implies a spatially symmetric relationship among all constituent defects. The much higher binding energy of $2V_O^{\cdot\cdot}4Gd'_{Ce}$ than $1V_O^{\cdot\cdot}2Gd'_{Ce}$ also indicates an intrinsic trend for cluster growth. The defect and binding energy of clusters, formed by more $V_O^{\cdot\cdot}$ and associated dopants, can be calculated in a similar way. Nevertheless, we can alternatively explain the cluster formation in terms of the intrinsic force generated from the defect-defect interaction, i.e., the interaction between an existing defect cluster and another newly enrolled defect. It is found that the newly evolved $V_O^{\cdot\cdot}$ prefers to locate along ⟨110⟩/2 with respect to its nearest $V_O^{\cdot\cdot}$. Figure 3(d) represents the most stable cluster constructed by three $V_O^{\cdot\cdot}$, which are shaped into an isosceles triangle with two equal edges along ⟨110⟩/2, forming an interior angle of 120°, and the lattice vector of its subtense being ⟨112⟩. All dopants occupy the sites satisfying the aforementioned criterion.

As the cluster grows to $4V_O^{\cdot\cdot}8Gd'_{Ce}$, a symmetric tetrahedron will be formed [Fig. 3(e)]. The three faces of the tetrahedron are constructed by three congruent isosceles triangles [the same one as shown in Fig. 3(d)]. This suggests a possible growth mechanism for defect clusters as a result of the formation of isosceles triangle units in the fluorite lattice. In other words, it is anticipated that all stable clusters, regardless of sizes, may be constructed with the same basic structures. This hypothesis has been verified by defect energy calculations of clusters growing up to $5V_O^{\cdot\cdot}10Gd'_{Ce}$ [Fig. 3(f)]. The newly

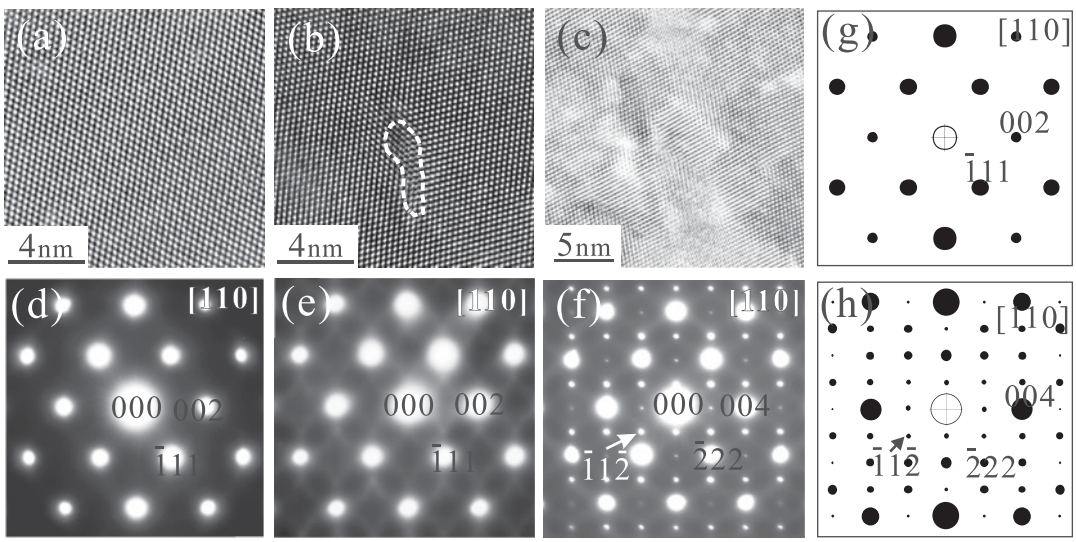

FIG. 1. HRTEM images of (a) 10GDC, (b) 20GDC, and (c) 50GDC. (d)–(f) are the corresponding SAED patterns. Computer-simulated diffraction patterns of F- and C-type structures observed along the [110] zone axis are shown in (g) and (f), respectively.

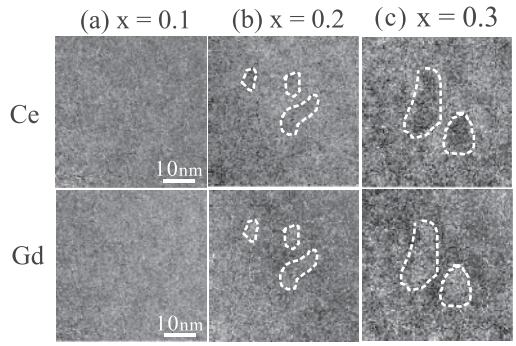

FIG. 2. EFTEM elemental maps of Ce and Gd of $Ce_{1-x}Gd_xO_{2-x/2}$ samples with (a) $x = 0.1$, (b) $x = 0.2$, (c) $x = 0.3$, illustrating the volume fraction of domains as a function of dopant concentration.

evolved $V_O^{\cdot\cdot}$ will occupy the site along $\langle 110 \rangle /2$ in relation to its nearest $V_O^{\cdot\cdot}$ in the existing tetrahedron structure, and meanwhile be involved in shaping the unique isosceles triangle with the next-nearest $V_O^{\cdot\cdot}$. If the cluster grows up to $6V_O^{\cdot\cdot}12Gd'_{Ce}$, a distinct symmetric configuration, designated as a dumbbell structure, appears [Fig. 3(g)]. The highly symmetric dumbbell structure cannot only be constructed from six congruent isosceles triangles [Fig. 3(d)], but also can be described as consisting of two congruent tetrahedrons [Fig. 3(e)], symmetrically interlocked by sharing one tetrahedral edge. Owing to the nonplanar separating vectors of constituent $V_O^{\cdot\cdot}$, the two congruent tetrahedrons are twisted along the sharing tetrahedral edge. Such a three-dimensionally symmetric and convergent structure implies a way for defect evolution as

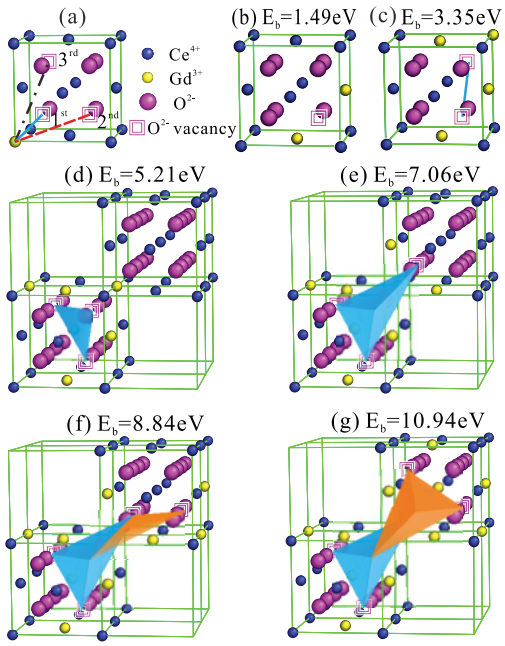

FIG. 3. (Color) (a) Oxygen vacancies at the first, second, and third neighbor site with respect to a dopant cation (Gd^{3+}) in the ceria fluorite structure. Defect clusters of (b) $1V_O^{\cdot\cdot}2Gd'_{Ce}$, (c) $2V_O^{\cdot\cdot}4Gd'_{Ce}$, (d) $3V_O^{\cdot\cdot}6Gd'_{Ce}$, (e) $4V_O^{\cdot\cdot}8Gd'_{Ce}$, (f) $5V_O^{\cdot\cdot}10Gd'_{Ce}$, (g) $6V_O^{\cdot\cdot}12Gd'_{Ce}$ with lowest defect energy and highest binding energy, compared to other defect clusters with the same number of defects.

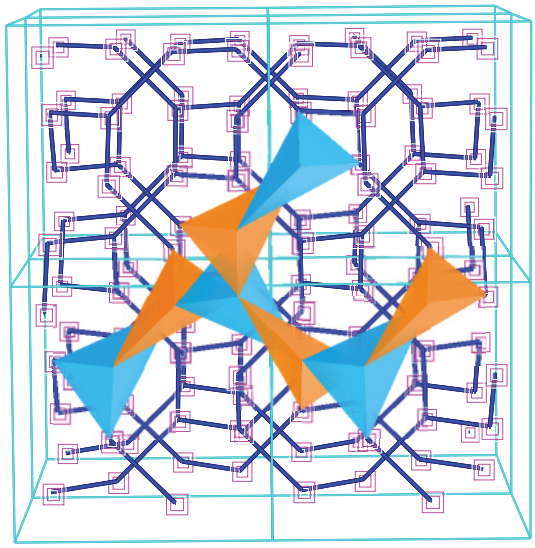

FIG. 4. (Color) Oxygen vacancies in a C-type lattice, with other ions omitted for clarity. Similar dumbbell structures as those shown in Fig. 2(g) are designated by two congruent edge-sharing tetrahedrons.

a function of cluster size. Based on the analysis of cluster growth in the F-type structure, it is necessary to investigate the evolution to the C-type structure to comprehensively explore the mechanism of cluster growth and the related pathway of phase transformation.

Figure 4 exhibits only $V_O^{\cdot\cdot}$ in the C-type lattice, with all other ions omitted for clarity. Note that any three adjacent $V_O^{\cdot\cdot}$, the closest two $V_O^{\cdot\cdot}$ aligning along $\langle 110 \rangle /2$ (connected by the blue lines), can form an isosceles triangle similar to the one in Fig. 3(d). With more nearby $V_O^{\cdot\cdot}$, similar unique structures as isosceles triangles, tetrahedrons, and dumbbells represented in Fig. 3 can be observed. Note that these dumbbells can be connected together and occupy all $V_O^{\cdot\cdot}$ sites in the C-type lattice, simply by coordinated spatial rotation due to the nonplanar separation of $\langle 110 \rangle /2$ lattice vectors. Therefore, the dumbbell structure described here may be regarded as the basic building block to construct the $V_O^{\cdot\cdot}$ sublattice in the C-type structure.

Quantitatively, defect clusters containing one to six $V_O^{\cdot\cdot}$ are compared in terms of the total binding energy in Fig. 5(a), in which the binding energy tends to increase with cluster size. This tendency suggests the higher stability of larger clusters and thus indicates an intrinsically attractive interaction

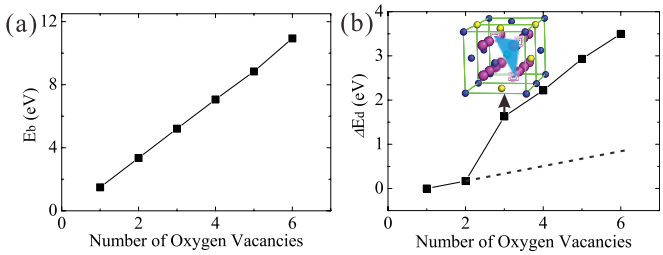

FIG. 5. (Color) (a) Binding energy (E_b) and (b) defect energy differences (ΔE_b) as a function of the number of oxygen vacancies in defect clusters.

among nearby defects, leading to the cluster growth. Different configurations of clusters with the same number of constituents have also been investigated. The defect energy difference (ΔE_d) between clusters with the lowest (structures are shown in Fig. 3) and the second lowest defect energy (not shown here) $\Delta E_d = E_{\text{2ndlowest}} - E_{\text{lowest}}$ was calculated [Fig. 5(b)]. When defect clusters are small (e.g., containing one or two $V_O^{\cdot\cdot}$), there are no significant differences in the defect energy, suggesting that all types of clusters have a similar probability of formation within the fluorite matrix. Nevertheless, when the cluster grows up to $3V_O^{\cdot\cdot}6Gd'_{Ce}$, there is a jump in the energy difference [denoted by the arrow in Fig. 5(b)], indicating a strong tendency to form this unique cluster. Beyond this critical point, the defect energy difference linearly increases with cluster size. Thus the $3V_O^{\cdot\cdot}6Gd'_{Ce}$ cluster may be a critical arrangement for cluster growth. Otherwise, a similar linear increase as that of smaller clusters should be anticipated [see the dashed line in Fig. 5(b)].

In light of the above analyses of cluster growth in F-type structures and spatial distributions of $V_O^{\cdot\cdot}$ in C-type structures, the rationalization for the phase transformation from the F- to C-type structure on the atomic scale through defect cluster growth follows. The substitution of Gd^{3+} for Ce^{4+} in the ceria lattice creates charge-compensating $V_O^{\cdot\cdot}$. At low doping levels (very small deviations from stoichiometry), defects are randomly distributed with few interactions.[1,7] As the doping level increases, the concentration of defects increases, and defect-defect interactions are expected. As two adjacent $V_O^{\cdot\cdot}$ aggregate, they will occupy the sites separated by $\langle 110 \rangle /2$. From this nucleus, an isosceles triangle structure [Fig. 3(d)] will be formed, with another nearby $V_O^{\cdot\cdot}$ aggregating. Beyond the critical point, defect clusters may continuously grow in terms of the formation of the basic stable structures, following the criterion demonstrated in Fig. 3. With up to six $V_O^{\cdot\cdot}$, a distinct symmetric dumbbell structure will form, which can act as the building block for larger cluster formation. Such formation of stable and ordered structures will provide the possible driving force for the aggregation and segregation of dopants and $V_O^{\cdot\cdot}$, leading to domain formations.[14,22,23] Since the $V_O^{\cdot\cdot}$ ordering is generally associated with cation ordering,[24] the enhanced $V_O^{\cdot\cdot}$ ordering in the net of dumbbell structures will increase the ordering level of accompanied dopants. The combination of short-range ordering of dumbbell structures (i.e., nanosized domain) will evolve into long-range ordering (i.e., superstructure) and subsequently develop into the entire ordering level in fluorite ceria. This ordering enhancement has been verified by both the appearance of diffuse scatterings and the electron energy-loss spectroscopy (EELS) analyses.[22,23] The domain growth, in terms of the formation of a series of dumbbell structures, will facilitate the phase transformation and gradually evolve into similar lattice sites of C type. The domain structure may hence be considered as an intermediate state between the F- and C-type structures. This mechanism may also work for other oxygen-deficient fluorite materials in accomodating $V_O^{\cdot\cdot}$, ordering sublattice anions and interpenetrated cation arrays, and subsequently triggering the related phase transformation. The final point to be emphasized here is that the interpretation of F- to C-type phase transformation through ordered defect cluster evolution is mainly based on the deduction process with a combination of TEM observations and atomistic simulation analyses. Due to the limited evidence of such a transitional process, further studies to quantitatively characterize this phase transformation in terms of defect cluster growth are strongly recommended.

In summary, an examination of the defect cluster formation and evolution in the fluorite structure reveals that the binding energy of defect clusters in GDC will increase with cluster size. The oxygen vacancies in the fluorite lattice prefer to form a unique isosceles triangle structure. The defect cluster will grow in terms of the formation and combination of such unique structures and subsequently construct a dumbbell structure, which can act as the building block that dominates the structure evolution from F to C type. Therefore, the phase transformation has been established to occur at the atomic level through the defect cluster growth.

The authors appreciate the financial support from the Grant-in-Aid for Scientific Research of the Ministry of Education, Culture, Sports, and Technology, Japan, and from Global Research Center for Environment and Energy based on Nanomaterials Science, National Institute for Materials Science, Japan. Z.P.L. thanks G. Auchterlonie (University of Queensland, Australia) for experimental assistance and helpful discussion.

*Corresponding author: zhipeng@email.unc.edu; present address: Department of Physics and Astronomy, University of North Carolina, Chapel Hill, NC 27599-3255.

[1] O. T. Sorensen, J. Solid State Chem. **18**, 217 (1976).
[2] H. Arai, T. Kunisaki, Y. Shimizu, and T. Seiyama, Solid State Ionics **20**, 241 (1986).
[3] N. Q. Minh, J. Am. Ceram. Soc. **76**, 563 (1993).
[4] B. C. Steele and A. Heinzel, Nature (London) **414**, 345 (2001).
[5] M. Mogensen, N. M. Sammes, and G. A. Tompsett, Solid State Ionics **129**, 63 (2000).
[6] H. Inaba and H. Tagawa, Solid State Ionics **83**, 1 (1996).
[7] J. A. Kilner and C. D. Waters, Solid State Ionics **6**, 253 (1982).
[8] A. K. A. Pryde, S. Vyas, R. W. Grimes, J. A. Gardner, and R. Wang, Phys. Rev. B **52**, 13214 (1995).
[9] L. H. Schoenlein, L. W. Hobbs, and A. H. Heuer, J. Appl. Crystallogr. **13**, 375 (1980).
[10] F. Pietrucci, M. Bernasconi, A. Laio, and M. Parrinello, Phys. Rev. B **78**, 094301 (2008).
[11] J. A. Ball, R. W. Grimes, and D. W. Price, Modell. Simul. Mater. Sci. Eng. **13**, 1353 (2005).
[12] M. S. Khan, M. S. Islam, and D. R. Bates, J. Mater. Chem. **8**, 2299 (1998).
[13] F. Ye, T. Mori, D. R. Ou, A. N. Cormack, R. J. Lewis, and John Drennan, Solid State Ionics **179**, 1962 (2008).
[14] Z. P. Li, T. Mori, F. Ye, D. R. Ou, J. Zou, and J. Drennan, J. Chem. Phys. **134**, 224708 (2011).
[15] D. J. M. Bevan and R. L. Martin, J. Solid State Chem. **181**, 2250 (2008).

[16]Z. P. Li, T. Mori, F. Ye, D. R. Ou, J. Zou, and J. Drennan, Microsc. Microanal. **17**, 49 (2011).
[17]M. R. Welton and W. Barndt, J. Phys. C **15**, 5691 (1982).
[18]G. V. Lewis, and C. R. Catlow, J. Phys. C **18**, 1149 (1985).
[19]S. Vyas, R. W. Grimes, D. H. Gay, and A. L. Rohl, J. Chem. Soc. Faraday Trans. **94**, 427 (1998).
[20]V. Bulter, C. R. A. Catlow, B. E. Fender, and J. H. Harding, Solid State Ionics **8**, 109 (1983).
[21]T. Mori, T. Kobayashi, Y. Wang, J. Drennan, T. Nishimura, J. G. Li, and H. Kobayashi, J. Am. Ceram. Soc. **88**, 1981 (2005).
[22]D. R. Ou, T. Mori, F. Ye, J. Zou, G. Auchterlonie, and J. Drennan, Phys. Rev. B **77**, 024108 (2008).
[23]Z. P. Li, T. Mori, G. Auchterlonie, J. Zou, and J. Drennan, Appl. Phys. Lett. **98**, 093104 (2011).
[24]S. G. Martin, M. A. A. Franco, D. P. Fagg, A. J. Feighery, and J. T. S. Irvine, Chem. Mater. **12**, 1729 (2000).